INDUCTION HEATING PROBLEMS FOR 2-D VECTOR ELECTROMAGNETIC CODE VALIDATIONS

Keith D. Paulsen and Daniel R. Lynch
Thayer School of Engineering
Dartmouth College, Hanover, NH USA

INDUCTION HEATING PROBLEMS FOR 2-D VECTOR ELECTROMAGNETIC CODE VALIDATIONS

Keith D. Paulsen and Daniel R. Lynch

ABSTRACT

Four problems in induction heating of lossy and non-lossy media are posed. The first consists of a simple two-region geometry which is amenable to analytic solution. Two possible boundary conditions are suggested, one of which requires the coupling of interior and exterior solutions (thus making a three region problem). The next two problems are "spin-offs" of the first where the geometry is modified in simple ways. We have found that while these alternate geometries are quite harmless in appearance, they nonetheless produce some very interesting and complex solutions which can be quite non-intuitive, especially when lossy and non-lossy media occur in combination. The final problem is an irregularly-shaped set of lossy regions placed inside a cylindrical induction heater. It is intended to be representative of induction heating of biological tissue as a cancer therapy. Some sample solutions are provided

PROBLEM STATEMENTS

Problem # 1

This problem consists of two concentric cylinders of dissimilar electrical properties as shown in Figure 1. Of interest is the electric field, **E**, produced in the plane. An analytic solution can easily be obtained by first solving for the z-directed (perpendicular to the plane of the paper) magnetic field, **H**, and differentiating in the appropriate way to obtain **E**. Two types of boundary conditions on the outer cylinder surface, R, are suggested: 1) a uniform magnetic field $\mathbf{H}(r,\phi) = H_o\hat{\mathbf{z}}$ and 2) a uniform surface current density $\mathbf{J}(r,\phi) = I_o\hat{\phi}$. It is quite easy to show that **H** is only a function of radial position in these cases and its solution can be found by matching boundary conditions at $r = a$ and $r = R$ (the inner and outer boundaries of the cylinders).

The first boundary condition results in a pure boundary value problem whose solution is

$$\mathbf{H}(r) = \begin{cases} AJ_o(k_1 r)\,\hat{\mathbf{z}} & r \le a \\ (BJ_o(k_2 r) + CY_o(k_2 r))\,\hat{\mathbf{z}} & a \le r \le R \end{cases} \tag{1}$$

where

J_o is the Bessel function of the first kind order zero

Y_o is the Bessel function of the second kind order zero

$k_n = \omega\sqrt{\mu\epsilon_n^*}; \quad n = 1, 2$

$\epsilon_n^* = \epsilon_n + i\sigma_n/\omega; \quad n = 1, 2$

$\hat{\mathbf{z}}$ is the direction perpendicular to the page

r is the radial coordinate

The constants A, B, and C are determined by ensuring continuity of **H** and $\frac{1}{k^2}\frac{\partial \mathbf{H}}{\partial r}$ at $r = a$ (in addition to the specified condition at $r = R$) which requires solving the system of equations

$$\begin{bmatrix} -J_o(k_1 a) & J_o(k_2 a) & Y_o(k_2 a) \\ -J_1(k_1 a)/k_1 & J_1(k_2 a)/k_2 & Y_1(k_2 a)/k_2 \\ 0 & J_o(k_2 R) & Y_o(k_2 R) \end{bmatrix} \begin{Bmatrix} A \\ B \\ C \end{Bmatrix} = \begin{Bmatrix} 0 \\ 0 \\ H_o \end{Bmatrix} \tag{2}$$

where

J_1 is the Bessel function of the first kind order one

Y_1 is the Bessel function of the second kind order one

a is the radius of the inner cylinder

R is the radius of the outer cylinder

H_o is the imposed magnetic field at R.

The quantity of interest, **E**, is then

$$\mathbf{E}(r) = \frac{1}{i\omega\epsilon^*}\frac{\partial H_z}{\partial r}\hat{\phi} \tag{3}$$

which becomes

$$\mathbf{E}(r) = \begin{cases} -\frac{k_1}{i\omega\epsilon_1^*} A J_1(k_1 r)\,\hat{\phi} & r \le a \\ -\frac{k_2}{i\omega\epsilon_2^*}(B J_1(k_2 r) + C Y_1(k_2 r))\,\hat{\phi} & a \le r \le R \end{cases} \tag{4}$$

The second outer boundary condition – imposing **J** – requires the coupling of interior and exterior solutions such that the discontinuity in **H** across the outer boundary is equal to **J**. In this case **H** can be written as

$$\mathbf{H}(r) = \begin{cases} A J_o(k_1 r)\,\hat{\mathbf{z}} & r \le a \\ (B J_o(k_2 r) + C Y_o(k_2 r))\,\hat{\mathbf{z}} & a \le r \le R \\ D H_o(k_3 r)\,\hat{\mathbf{z}} & R \le r \end{cases} \tag{5}$$

where H_o is the Hankel function of the first kind order zero and the other definitions remain as before. Note i runs from 1 to 3 indicating the involvement of the exterior solution (i.e. $R \le r$). The system of equations that need to be solved in order to determine the constant coefficients is

$$\begin{bmatrix} -J_o(k_1 a) & J_o(k_2 a) & Y_o(k_2 a) & 0 \\ -J_1(k_1 a)/k_1 & J_1(k_2 a)/k_2 & Y_1(k_2 a)/k_2 & 0 \\ 0 & J_o(k_2 R) & Y_o(k_2 R) & -H_o(k_3 R) \\ 0 & J_1(k_2 R)/k_2 & Y_1(k_2 R)/k_2 & -H_1(k_3 R)/k_3 \end{bmatrix} \begin{Bmatrix} A \\ B \\ C \\ D \end{Bmatrix} = \begin{Bmatrix} 0 \\ 0 \\ I_o \\ 0 \end{Bmatrix} \tag{6}$$

where H_1 is the Hankel function of the first kind order one. **E** is obtained from (3) as before such that

$$\mathbf{E}(r) = \begin{cases} -\frac{k_1}{i\omega\epsilon_1^*} A J_o(k_1 r)\,\hat{\mathbf{z}} & r \le a \\ -\frac{k_2}{i\omega\epsilon_2^*}(B J_o(k_2 r) + C Y_o(k_2 r))\,\hat{\mathbf{z}} & a \le r \le R \\ -\frac{k_3}{i\omega\epsilon_3^*} D H_o(k_3 r)\,\hat{\mathbf{z}} & R \le r \end{cases} \tag{7}$$

In our work, we are interested in the heating of biological tissue; hence, we have explored this problem using combinations of electrical properties which are representative of tissues. Typically, we take the outer cylinder radius as 25 cm and the inner cylinder radius as 12 cm as shown in Figure 1 (we have also used 10 cm and 15 cm for the inner cylinder radius). The frequencies of interest have been 10, 13, 70, 100 and 130 MHz. As examples, we suggest trying various combinations of the electrical properties shown in Table 1. One combination which we have found as a good starting point is muscle surrounded lung ($\epsilon_r = 40$, $\sigma = .35\,\Omega^{-1}m^{-1}$). Sample solutions can be found in [1].

Problem # 2

This problem is a slight variation on Problem 1 where the inner cylinder is moved "off-center" as shown in Figure 2. The same boundary conditions described for problem 1 can be used. In this case, **H** and **E** become functions of the azimuthal angle as well as radius. We find some particularly interesting solutions when the inner cylinder is lossless while the outer cylinder is lossy. In addition to trying various combinations of the electrical properties listed in Table 1, we suggest parameters which result in – $(|k_2|R)^2 = 6 \rightarrow 12.5$, $|k_1|^2 = 10|k_2|^2$, $\sigma_2/\omega\epsilon_2 = .2 \rightarrow 2$, $\sigma_1/\omega\epsilon_1 = 0$ – as cases which produce some intriguing solutions (subscripts "1" and "2" correspond to the inner and outer cylinders, respectively).

Figure 3 shows a sample solution computed with the numerical method described below. The data plotted are the real and imaginary components of the computed complex amplitude of the electric field. Vector lengths are scaled proportionally to their strength. When a node lies on an interface between electrically distinct regions, two vectors are drawn reflecting the jump discontinuity in the electric field at that location. The case shown has $(|k_2|R)^2 = 6.25$, $|k_1|^2 = 10|k_2|^2$, $\sigma_2/\omega\epsilon_2 = 20$, $\sigma_1/\omega\epsilon_1 = 0$. Another example where $(|k_2|R)^2 = 12.5$, $|k_1|^2 = 10|k_2|^2$, $\sigma_2/\omega\epsilon_2 = .2$ and $\sigma_1/\omega\epsilon_1 = 0$ can be found in [2].

Problem # 3

This problem represents another variation on the geometry of Problem 1. In this case the outer cylinder is split into semi-circular regions of distinct electrical properties as illustrated in Figure 4. Outer boundary conditions remain the same. Cases that we recommend as starting points are bone in combination with air and water, and lung in combination with muscle. Figure 5 show a sample solution where $(|k_2|R)^2 = 45.944$, $|k_1|^2 = 0.44548|k_2|^2$, $\sigma_2/\omega\epsilon_2 = 1.6960$, $\sigma_1/\omega\epsilon_1 = 1.5728$ (subscript "1" corresponds to the bottom half of the cylinder in Fig 4). The data plotted have the same format as that described above for Problem 2. Another example (air/bone case) can be found in [2].

Problem # 4

This problem represents a realistic 2-D model of a cancer patient cross-section placed inside an induction heating coil. The geometry is shown in Figure 6 and the various tissue properties are given in Table 1. While tissue electrical properties do change with frequency, an interesting exercise from a software validation perspective is to use the properties listed in Table 1 for various frequencies. We recommend 10, 13, 70, 100 and 130 MHz as reasonable examples. Obviously, there is no analytical solution for this problem, but we have achieved excellent code-to-code agreements. Figure 7 shows a sample solution computed for the 130 MHz case where air is used as the medium surrounding the patient (Note that the electrical properties of each tissue were taken from the 13 MHz columns in Table 1 for the simulation shown). The data plotted have the same format as that described for Problem 2. Other example solutions of this type can be found in [1].

NUMERICAL METHOD

The example solutions shown in Figs 3, 5, and 7 were obtained by the finite element method. Computation was perfomed directly on the vector PDE for the electric field. An extended weak form has been implemented and the details of this formulation can be found in [1] for the time-domain and [2] for the frequency-domain. We find that the conventional double-curl equation on simple scalar bases leads to parasitic solutions which overwhelm the computation in Problems 2, 3, and 4. These difficulties do not appear to arise in Problem 1.

Since closed-form solutions are not readily available for Problems 2, 3, and 4, considerable effort has been devoted to code-to-code validations. The solutions shown have been benchmarked against a scalar magnetic field formulation (which is subsequently differentiated to obtain the electric field) and excellent agreement has been achieved in both boundary-value and hybrid formats. Further, independent time-stepping results, once the dynamic steady-state has been reached, agree favorably with their direct frequency-domain matrix solution counterparts. These validation experiences have been carefully documented in [1,2].

COMPUTATIONAL EFFORT

All calculations have been made on a VAXstation 3200 with 16 megabytes of core memory using single-precision Fortran. Solutions have been obtained with direct LU decomposition of the banded matrices resulting from the algebra produced by the finite element formulation. Run-times (including data I/O, matrix assembly, etc.) of 3, 20, and 7.5 minutes have been recorded for the solutions in Figure 3 (Problem 2), Figure 5 (Problem 3), and Figure 7 (Problem 4), respectively.

The mesh in Figure 2 consists of 1069 nodes (2020 elements). The computed bandwidth is 171 which results in a 2138×171 complex matrix requiring 2.9 megabytes of storage space. The mesh in Figure 3 is composed of 1501 nodes (1500 elements) yielding a bandwidth of 479 and a 3002×479 complex matrix requiring 11.5 megabytes of memory. Both grids were generated using automatic meshing algorithms; however, only in the former case was bandwidth reduction attempted. The grid in Figure 6 consists of 1325 nodes (1449 elements). The bandwidth in this case is 247; hence, the resulting 2650×247 complex matrix occupies 5.2 megabytes of storage space. These computational meshes are available on request.

SUMMARY

We have found the above EM problems to be very useful for validating 2-D vector codes which solve directly for the electric field. These problems require algorithms that contain essentially all the ingredients needed for full 3-D EM calculations (e.g vector quantities, interface conditions, unbounded fields, etc). Thus, they afford an opportunity to gain confidence and experience with computational EM on 2-D problems before embarking on 3-D calculations. The geometries are simple but nevertheless result in some interesting and complex solutions. While known solutions cannot be obtained for all the problems described, we have achieved code-to-code agreement for these problems and would gladly share our experiences and solutions with interested parties. Some sample solutions have been included.

REFERENCES

1. DR Lynch and KD Paulsen, "Time-Domain Integration of the Maxwell Equations on Finite Elements," *IEEE Trans Antennas and Propagation* (in review).

2. KD Paulsen and DR Lynch, "Elimination of Vector Parasites in Finite Element Maxwell Solutions," *IEEE Trans Microwave Theory and Techniques* (in review).

TABLE I

Electrical properties of tissue

	13 Mhz		70 Mhz	
Tissue	ε_r	σ ($\Omega^{-1}m^{-1}$)	ε_r	σ ($\Omega^{-1}m^{-1}$)
Air	1	.00	1	.00
Bladder	50	1.44+ , .002*	50	1.44+ , .002*
Bone	28	.20	10	.02
Bone marrow	200	.65	7	.04
Fat	28	.20	10	.21
Feces	113	.60	113	.60
Intestine	80	.41	80	.57
Kidney	330	.80	89	1.00
Muscle	122	.60	85	.802
Tumor	122	.60	85	.802
Water	70	.00	70	.00

μ was taken as equal to the magnetic permeability of free space for all tissues.

ε_r = relative dielectric constant

σ = electrical conductivity

\+ = urine-filled

* = flushed, non-ionized water

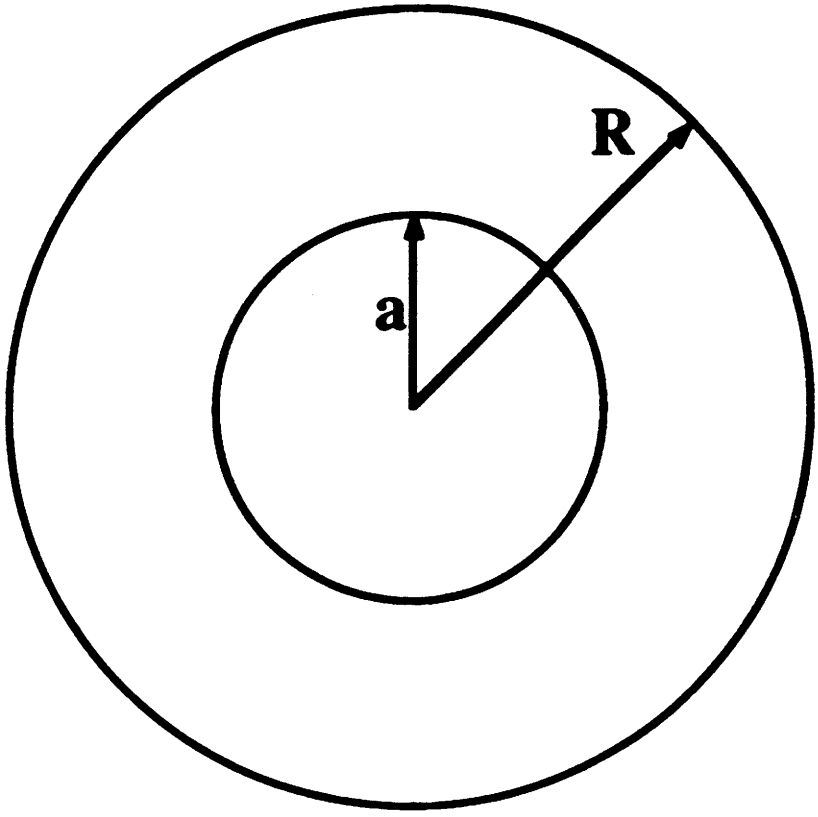

Figure 1. Geometry for Problem # 1 – two concentric cylinders having distinct electrical properties. Suggested values are $R = 25\,cm$ and $a = 12\,cm$.

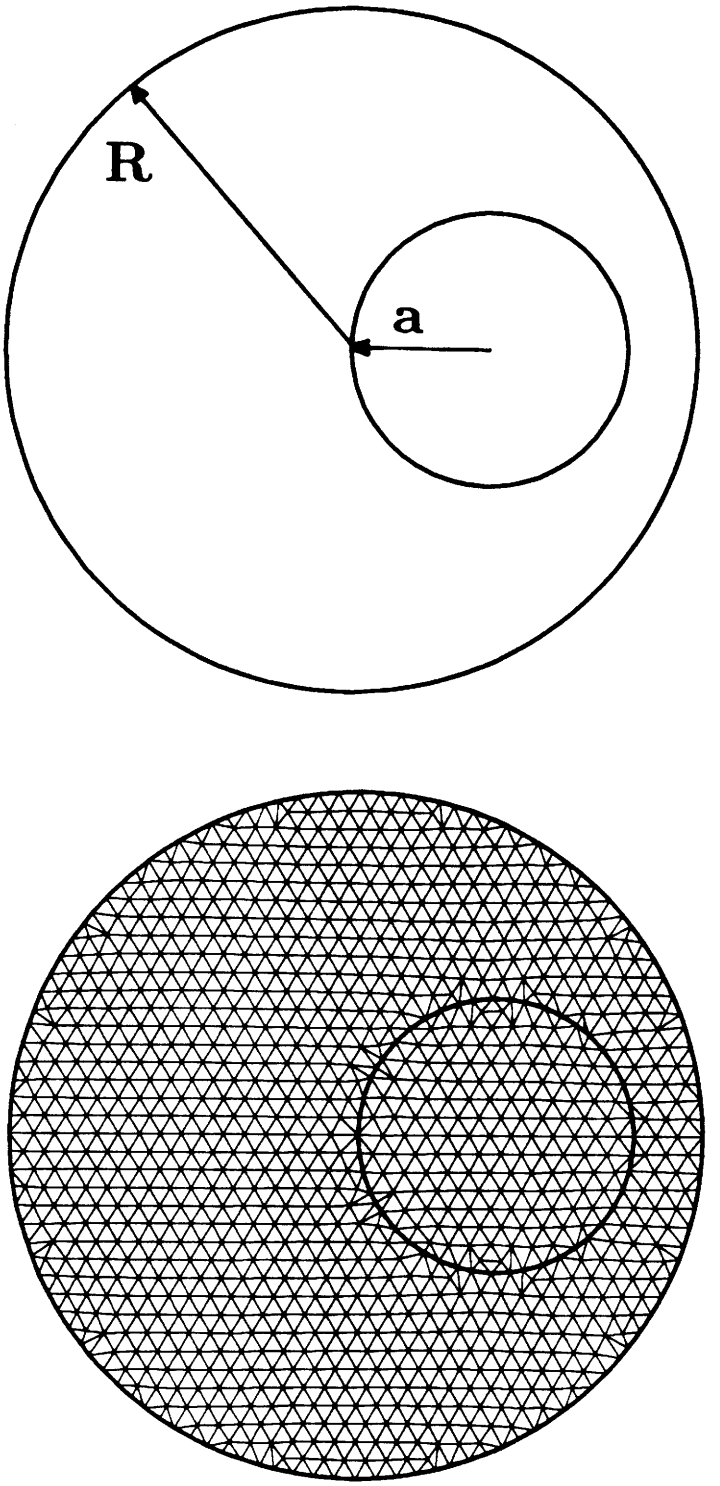

Figure 2. Geometry for Problem # 2 – an off-center inner cylinder contained within an outer cylinder each of which have dissimilar electrical properties (top). $R = 25\,cm$ and $a = 10\,cm$. Center of inner cylinder located at (10,0). Finite element mesh used to compute the solution in Fig 3 is shown (bottom).

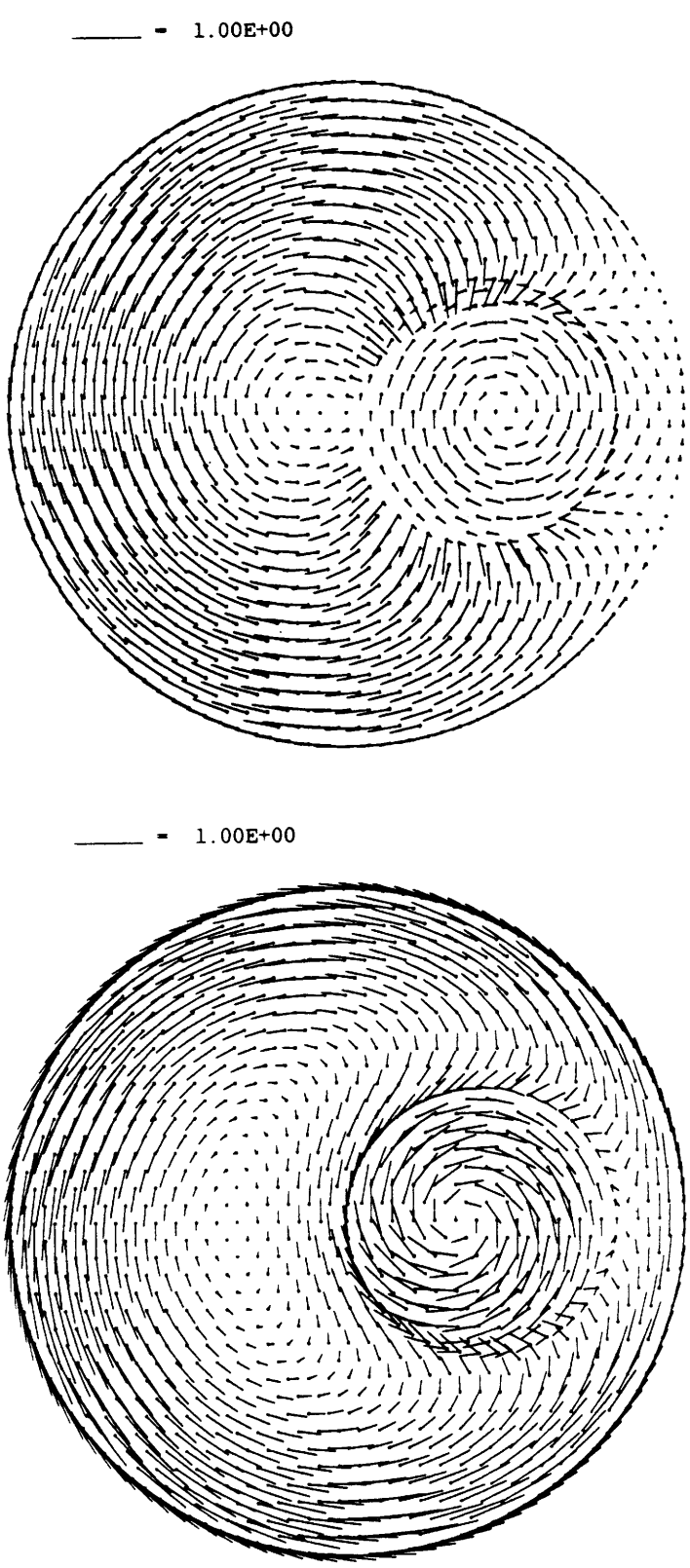

Figure 3. Sample solution computed on the grid in Fig 2. Vector plots of $Re(\mathbf{E})$ (top) and $Im(\mathbf{E})$ (bottom) are shown. Vector lengths are proportional to strength (max scaled to unity). See text for electrical properties of each region.

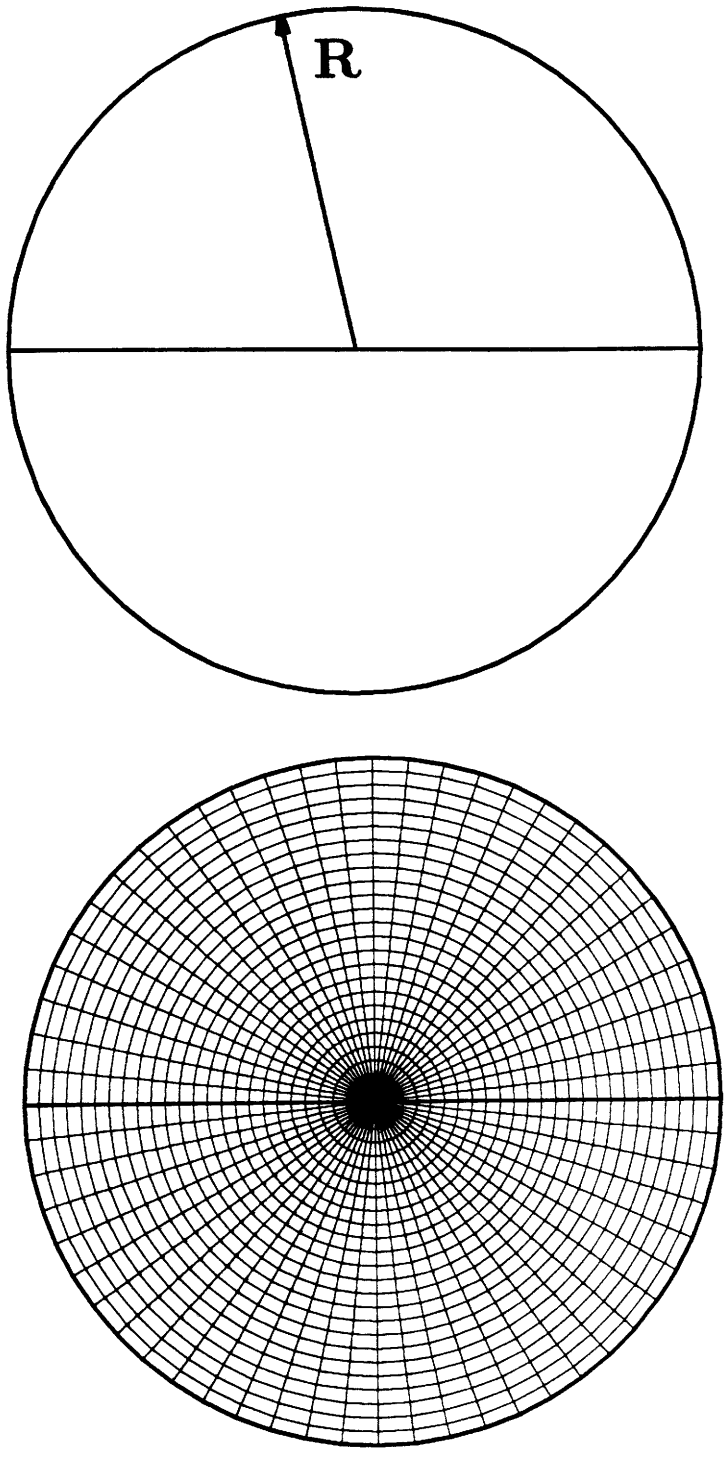

Figure 4. Geometry for Problem # 3 – a single cylinder split into two semi-circular regions of different electrical properties (top). $R = 25\,cm$. Finite element mesh used to compute the solution in Fig 5 is shown (bottom).

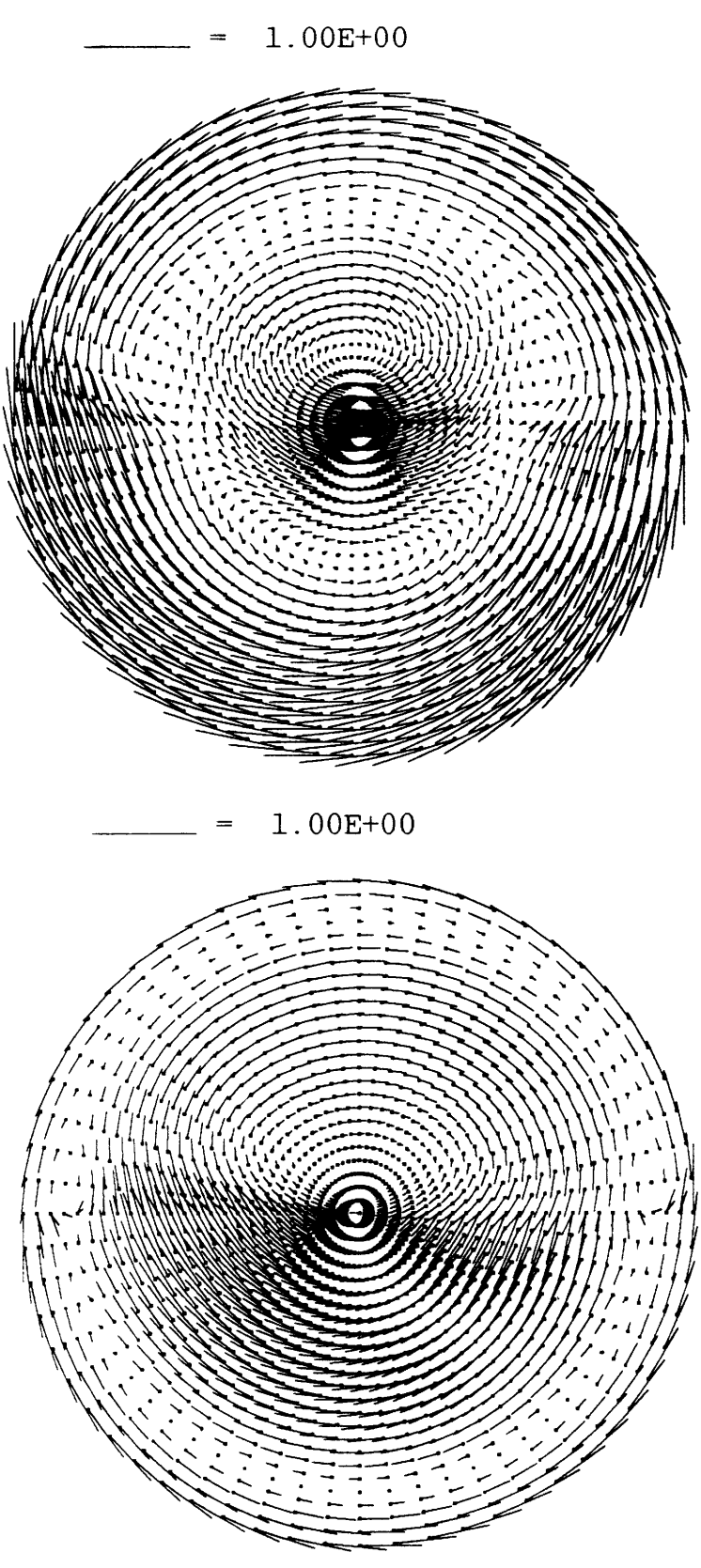

Figure 5. Sample solution computed on the grid in Fig 4. Vector plots of $Re(\mathbf{E})$ (top) and $Im(\mathbf{E})$ (bottom) are shown. Vector lengths are proportional to strength (max scaled to unity). See text for electrical properties of each region.

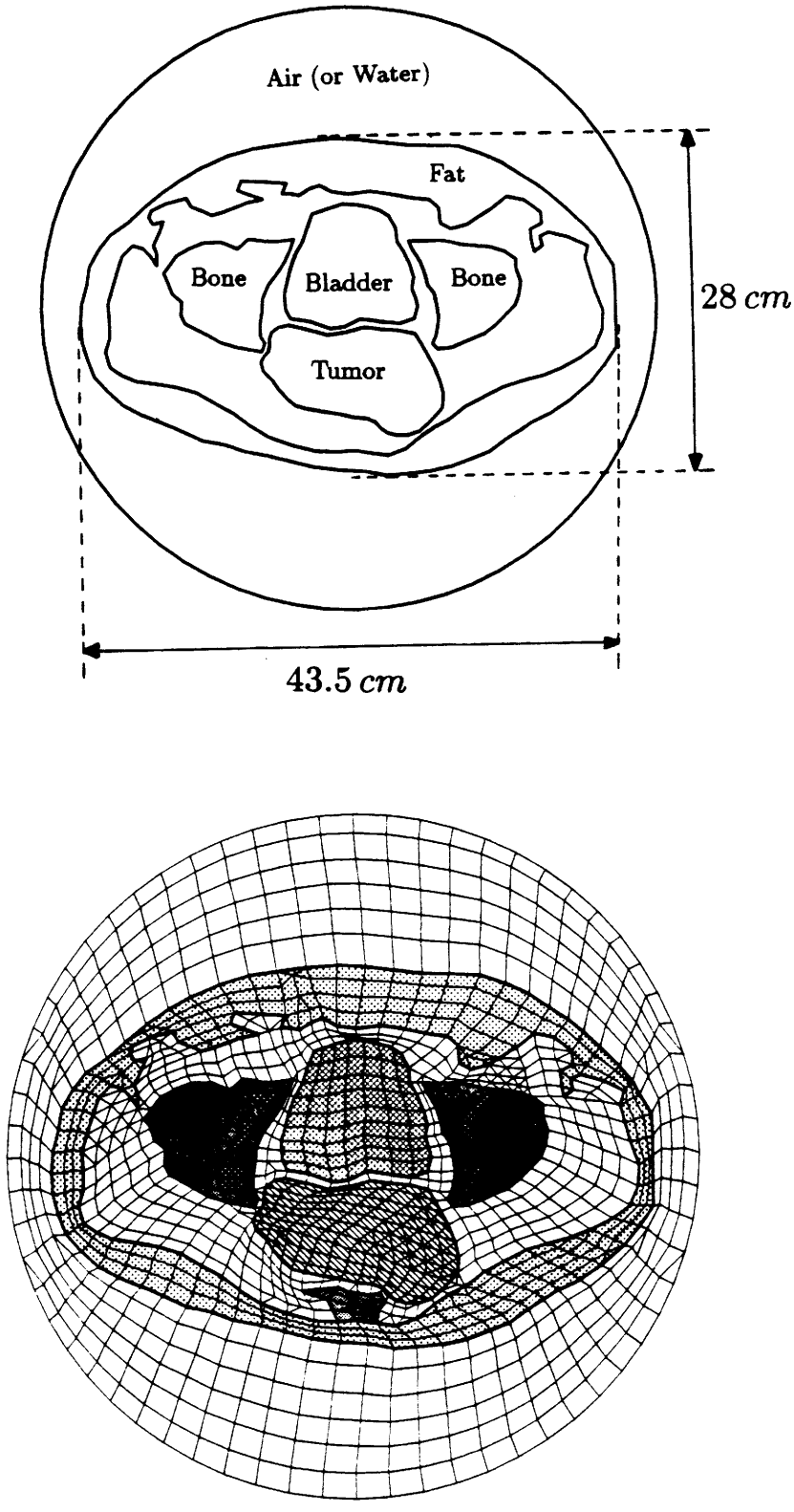

Figure 6. Geometry for Problem # 4 – cross-section of a cancer patient placed inside an induction coil (top). The radius of the coil is 25 cm. Finite element mesh used to compute the solution in Fig 7 is shown (bottom).

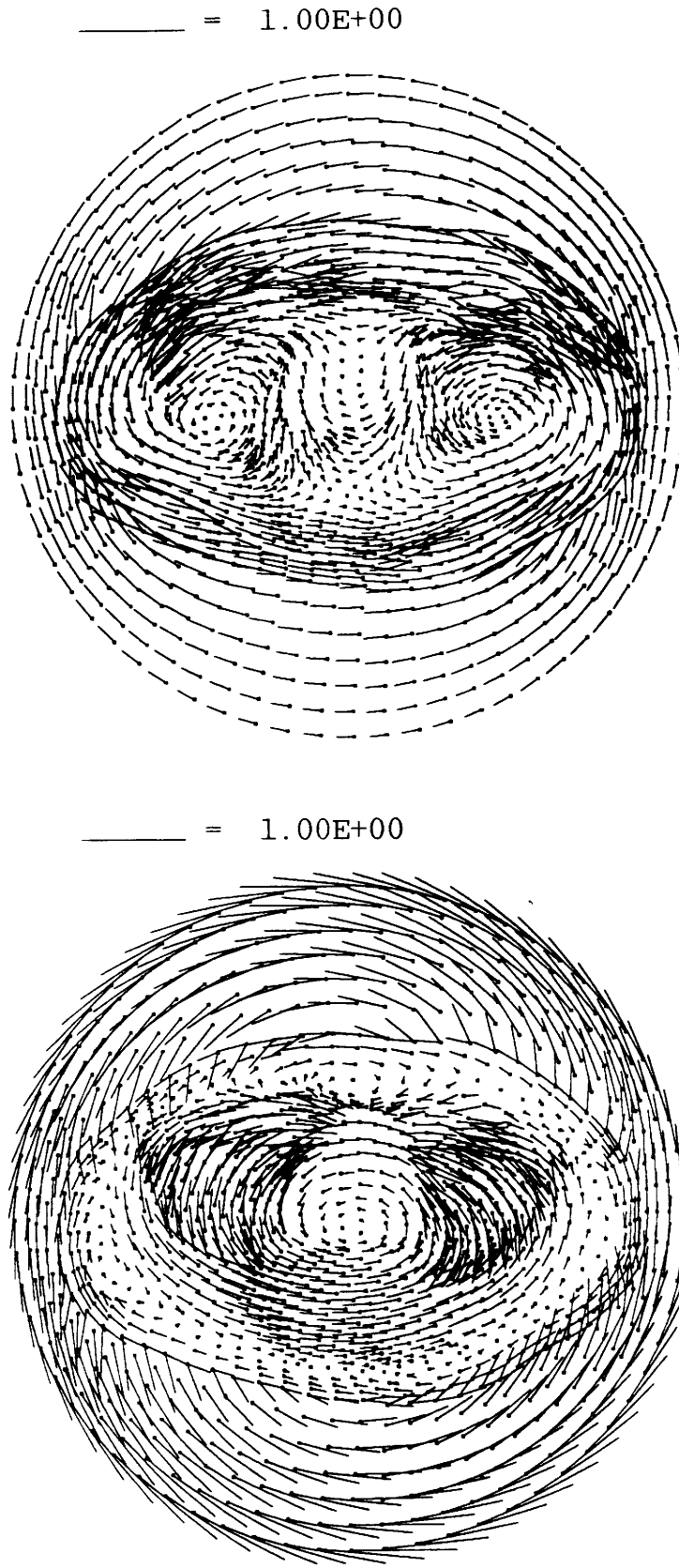

Figure 7. Sample solution computed on the grid in Fig 6. Vector plots of $Re(\mathbf{E})$ (top) and $Im(\mathbf{E})$ (bottom) are shown. Vector lengths are proportional to strength (max scaled to unity). See text for electrical properties of each region.